P53

2D Quantitative Imaging by Elastic Full Waveform Inversion: Application to a Physical Scale Model

F. Bretaudeau* (Laboratoire Central des Ponts et Chaussee(LCPC)), D. Leparoux (LCPC), R. Brossier (LGIT), S. Operto (Geoazur) & O. Abraham (LCPC)

SUMMARY

Quantitative imaging of the first meters of the underground with seismic methods is an important challenge for many applications. This task is difficult because of heterogeneity, strong attenuation, low frequency content and large dominance of surface waves in the data. Tomography, migration, and dispersion analysis of surface wave are not efficient in all contexts. Elastic full waveform inversion was developed for crustal imaging but has a great potential for near surface applications as it could help to image very heterogeneous media by exploiting the whole complexity of the seismograms.
We try here to (1) understand how behaves this method on near surface context, and (2) anticipate on the field application. We use for that a simultaneous approach by applying the waveform inversion on a simple three layer medium from synthetic data obtained by numerical modeling, and from experimental data obtained by small scale modeling. We present the small scale model, the acquisition of synthetic and experimental data, and we present an inversion result.
Images of the Vp and Vs parameters are reconstructed. Both lateral and vertical variations are well determined. Images from synthetic and experimental data can be compared. The results are similar but we identify differences related to noise.

Introduction

Quantitative imaging of the first meters of the underground in 2D or 3D with seismic methods is an important challenge for plenty of applications as varied as soil characterisation in geotechnics, landscape management, environement or archaeology. But heterogeneity and strong attenuation of the near surface useally provide seismic data dominated by energetic and complex surface waves. Because refracted and reflected body waves are sometimes difficult to pick up in this contexts, near surface heterogeneities can be difficult to image using surface tomography or migration processing. Morover, dispersion analysis of surface waves (SASW) is not efficient in presence of strong lateral variations or very complex structures. Full waveform imaging methods, developped in time domain (Tarantola, 1984) as well as in frequency domain (Pratt, 1999), are currently subject of intensive research in oil prospecting and more generally for crustal imagery, but have been very few investigated for near surface applications (Gélis et al., 2007). Full waveform inversion (FWI) in the elastic approximation could help to take advantage of the whole complexity of the near surface seismic data by taking into account reflected, refracted and surface waves, but also all near surface diffractions of P- S- and surface waves. However, before the difficult task of applying this method to field data, it is necessary to (a) evaluate how behaves the imagery process on near surface context, and (b) evaluate how can behave the method on real noisy data and identify the origins of the difficulties ?

We present herein on a simple 2D case how elastic waveform inversion in the frequency domain allows quantitative reconstruction of near surface heterogeneities. We choose a configuration where the reconstruction is difficult because the layer interfaces are too deep and the impedance contrasts too weak to generate refracted waves or dispersive surface waves in the data. In this context, reflected body waves are mostly hidden by the surface wave wavefront making the migration processing inefficient.

The imagery test presented here involves synthetic data generated by a visco-elastic finite-element modeling algorithm (Brossier et al., 2008), and experimental data obtained on a similar medium thanks to small scale modeling with an laser-ultrasonic equipment dedicated to seismic data acquisition (Bretaudeau, 2010). In a first stage, we present how we generate the synthetics, how we obtain similar experimental data, and we compare them. In a second stage, we present the result of elastic waveform inversion from ideal synthetic data and from experimental ultrasonic data using waveform inversion algorithm developed by Brossier (2009). Then the results are discussed and the quantitative images provided from ideal synthetic data and real experimental are compared.

Numerical and experimental modeling of shallow seismic data

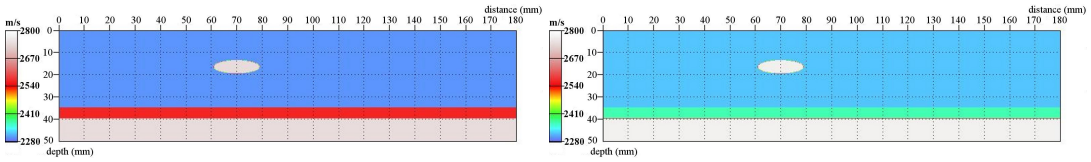

(a) V_P (b) V_S

Figure 1: V_P and V_S exact velocity models.

The study is based on a joint approach using a similar numerical and experimental medium. Indeed the 2D numerical medium presented on figure 1 is built using dimensions and visco-elastic properties of an epoxy-resin physical model. Both physical and synthetic media are composed of three layers with velocities that increase with depth from $V_P = 2300\,m.s^{-1}$ and $V_S = 1080\,m.s^{-1}$ to $V_P = 2740\,m.s^{-1}$ and $V_S = 1427\,m.s^{-1}$. The first layer is $35\,mm$ thick and contains an ellipsoidal higher velocity inclusion. The second layer is $5\,mm$ thick and the third layer simulates the infinite underground. The physical model is large enough on each edge ($L = 500\,mm$, $l = 400\,mm$, $h = 260\,mm$) to facilitate the boundary effects filtering and simulate a semi-infinite medium, but the numerical medium of figure 1 is built according to a

limited domain of $180\,mm$ long and $50\,mm$ depth that is the investigated part of the medium. The source signal is $100\,kHz$ Ricker wavelet.
For instance, these physical and numerical scales should simulate a real near surface scale with a scale factor of $1/2$ on velocities, $1/2000$ on frequencies and 1000 on distances. The real scale would therefore be $180\,m$ long and $50\,m$ depth, P-wave velocities would be between $1150\,m.s^{-1}$ and $1400\,m.s^{-1}$ while the S-waves would be between $540\,m.s^{-1}$ and $713\,m.s^{-1}$. The inclusion would be located at $15\,m$ depth and data spectrum would be around $50\,Hz$.
The same acquisition survey is used for both numerical and physical models. It is composed of 37 source points and 180 receiver points and spreads regularly all along the free surface.
The ultrasonic data set is obtained thanks to the MUSC laser-ultrasonic laboratory, recently developed in LCPC (Laboratoire Central des Ponts et Chausses) (Bretaudeau, 2010). The MUSC laboratory allows here to record surface seismic data set with a punctual ultrasonic source excited by a $100\,kHz$ Ricker wavelet, and to record the vertical particular displacement at the surface of the model thanks to non-contact laser interferometry. The positions of the source and receiver are controlled with an accuracy of $10\,\mu m$, and data are sampled at $10\,MHz$ ($dt = 0.1\,\mu s$). The ultrasonic seismogram obtained from shot position n°1 is presented on figure 2-a. On this example, preprocessing like band-pass filtering, noise removing, filtering and muting parasitic arrivals, has been applied. The seismogram highlights direct P and Rayleigh waves (1,2), very weak P- and S-wave reflected on deep interface (3-4), a Rayleigh wave diffraction (5) and a very weak P-wave diffraction (6). (5) and (6) are associated with the rigid inclusion laterally located between 60 and $80\,mm$ on the model figure 1. Time arrivals of reflected waves are difficult to pick because they are partially hidden by the Rayleigh wave. Second and third layers are too deep and attenuation is too high to record refracted waves. The dispersion diagram of figure 2-b shows that the deep layers are too deep to generate dispersion of the surface wave in the frequency range present in the data. In an other hand, we clearly see that the near surface inclusion generates a body wave diffraction, but above all an important Rayleigh wave diffraction that is difficult to put in relation with a quantitative information. In other words, all the informations concerning the investigated domain are present in the data but it is a priori not trivial to treat them by classical methods to get a quantitative image of the medium.

Synthetic data are calculated for the same sources and receivers positions with the visco-

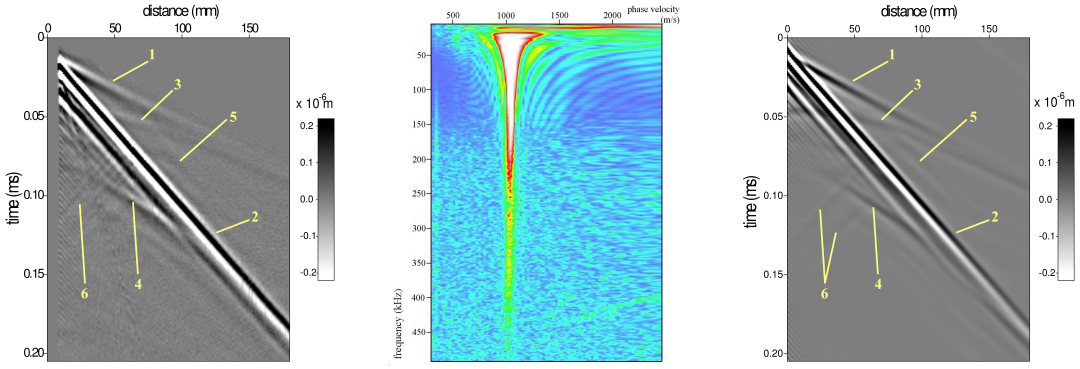

(a) Experimental seismogram from shot n°1. (1) direct P-wave, (2) Rayleigh wave, (3-4) P- and S- reflections, (5) P-wave diffraction by the inclusion, (6) Rayleigh wave diffraction

(b) Dispersion diagram extracted from a seismogram recorded far from the inclusion. Surface wave is not dispersive in the frequency range $30 - 400\,kHz$.

(c) Synthetic seismogram from shot n°1. All events observed in ultrasonic data are reproduced by numerical modeling. Time arrival and amplitudes are respected.

Figure 2: Synthetics and ultrasonic data

elastic frequency-domain finite-element discontinuous Galerkin modeling algorithm developed in Brossier (2009). The real source wavelet with true amplitude that penetrate in the model at

the point source location is determined using a linear optimisation as proposed by Pratt (1999). The misfit function between real and synthetic data calculated with the true medium is minimized by adjusting the source wavelet. The inverted wavelet is presented in figure 3-a and its Fourier transform in figure 3-b. This extracted wavelet reckon with the frequency bandwith $(30 - 200\,kHz)$ and the time response of the power amplifior and of the piezoelectric source, as well as the source coupling. Data are then calculated using this source wavelet and the same

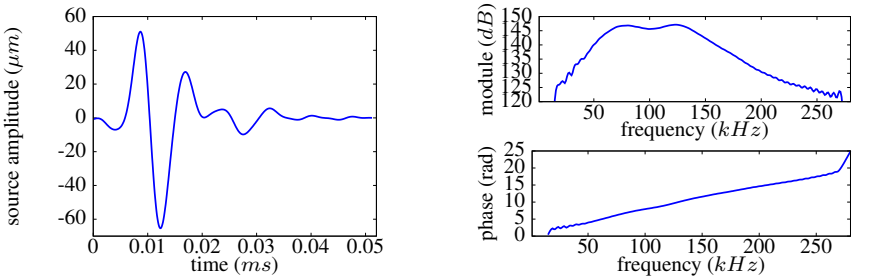

(a) Temporal signal

(b) Fourier transform of the real source wavelet

Figure 3: Real source wavelet at the point source location.

sampling parameters of those used for ultrasonic data. Synthetic data are presented on figure 2-c and can be compared with ultrasonic data of figure 2-a. P-wave, Rayleigh wave, body wave reflections, diffractions, and Rayleigh wave perturbations generated by the rigid inclusion are all reproduced respecting time arrivals and amplitudes. The main difference between synthetic and ultrasonic data is the absence of noise. Thus data sets can be exploited through the FWI process.

Waveform inversion results

The waveform inversion strategy we used is based on the frequency domain formulation proposed by Pratt and Worthington (1990). The algorithm (Brossier, 2009) is based on a iterative preconditioned conjugate-gradient optimisation and the forward solution is computed by the same finite-element code used to generate our synthetic data. Lot of authors (Pratt and Worthington, 1990; Pratt, 1999; Sirgue and Pratt, 2004) have shown this non-linear inverse problem can be resolved only if the initial model is robust enough and if the non-linearity is mitigated by introducing sequentially informations from the low to the high frequencies. Thus we start from the initial model presented figure 4-a,b that corresponds to a smoothed version of the true medium without the inclusion in the first layer. Then 14 frequencies are sequentially inverted from $29\,kHz$ to $156\,kHz$ with 5 iterations for each frequency. Therefore the corresponding wavelengths of Rayleigh wave are respectively from $35\,mm$ to $6.5\,mm$ when inclusion is located at depth between 15 and $20\,mm$.

Figures 4-c and d represent the final result obtained from synthetic data at the last frequency $(156\,kHz)$. The inclusion and deep layers are well localised and quantitatively imaged with an accuracy that decreases with depth. Artefacts and differences compared to the exact model are due to the unfavourable one side surface illumination and the lack of information from very low $(< 29\,kHz)$ and very high frequencies $(< 156\,kHz)$ in the inverted data. This result can be compared with those obtained with exactly the same strategy but from real ultrasonic data (figure 4-e,f). Result is globally similar but we notice several differences. Slight differences in amplitude of the parameters and in the size and location of imaged structure has been linked to slight differences between physical and numerical models. We also notice artefacts mainly concentrated nearby the free surface that are supposed to be related with higher non-linearity of the problem in this region which creates instability of the inversion when it is combined with noise.

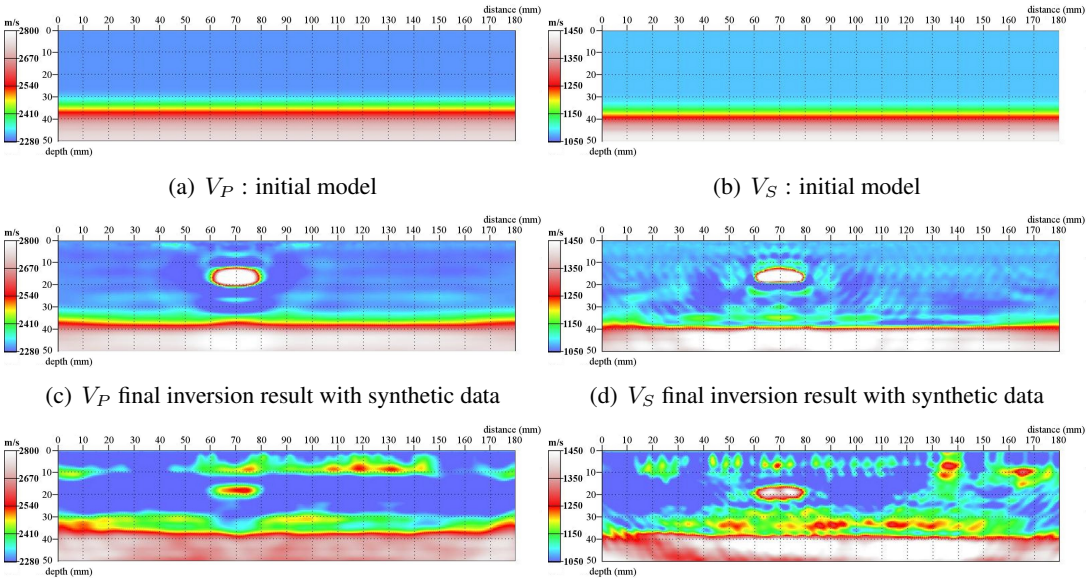

(a) V_P : initial model

(b) V_S : initial model

(c) V_P final inversion result with synthetic data

(d) V_S final inversion result with synthetic data

(e) V_P final inversion result with experimental data

(f) V_S final inversion result with experimental data

Figure 4: V_P and V_S velocity models obtained from sequential frequency-domain waveform inversion. (a) and (b) are initial models, (c) to (f) are final results obtained at $156\,kHz$. Theoretical imaging resolution is for V_P $\lambda_P/2 = 7.4\,mm$, and for V_S $\lambda_S/2 = 3.5\,mm$.

Conclusions

We have shown the potential of elastic FWI to quantitatively image complex near surface structures. We also identify any difficulties related to the method itself in this context, and difficulties related to the experimental conditions. Before to apply FWI on real field data, future works will have to concentrate on FWI behavior with dispersive media, with the optimisation of the inversion strategy, the determination of a robust initial model, and to find solutions to mitigate the instabilities caused by presence of noise.

Acknowledgements

This study was partly funded by the French ANR SEISCOPE and ACTENA.

References

Bretaudeau, F. [2010] Modélisation physique à échelle réduite pour l'adaptation de l'inversion des formes d'ondes sismiques au génie civil et à la subsurface.

Brossier, R. [2009] Imagerie sismique à deux dimensions des milieux visco-élastiques par inversion des formes d'ondes : développements méthodologiques et applications.

Brossier, R., Virieux, J., and Opertro, S. [2008] Parsimonious finite-volume frequency-domain method for (2-D) (P-SV)-wave modelling. *Geophysical Journal International*, **175**, 541–559.

Gélis, C., Virieux, J., and Grandjean, G. [2007] Two-dimensional elastic full waveform inversion using born and rytov formulations in the frequency domain. *Geophysical Journal International*, **168**(2).

Pratt, R. [1999] Seismic waveform inversion in the frequency domain, part 1: Theory and verification in a physical scale model. *Geophysics*, **64**(3), 888–901.

Pratt, R. and Worthington, M. [1990] Inverse theory applied to multi-source cross-hole tomography. i: Acoustic wave-equation method. *Geophysical Prospecting*, **38**(3), 298–310.

Sirgue, L. and Pratt, R. [2004] Efficient waveform inversion and imaging: A strategy for selecting temporal frequencies. *Geophysics*, **69**(1), 231–248.

Tarantola, A. [1984] Inversion of seismic reflection data in the acoustic approximation. *Geophysics*, **49**(8), 1259–1266.